Liquid coating by an elastic sheet

By BERTRAND SELVA, VIRGINIE DUCLAUX,
AND CHRISTOPHE CLANET[1]

[1] IRPHE, UMR 6594, 49 rue F. Joliot-Curie, BP 146, 13384 Marseille, France

We study the thickness h_∞ of a liquid film (dynamic viscosity μ) when deposited on a rigid surface by an elastic sheet (length L, bending stiffness B) moving at the relative velocity V. We first show experimentally that :

$$h_\infty \approx 0.065 L \left(\frac{\mu V L^2}{B} \right)^{3/4}$$

Theoretically, we approach this law with an extension of the Landau-Levich-Derjaguin problem.

1. Introduction

The deposition of a constant thickness liquid film (dynamic viscosity μ, density ρ, surface tension σ) on a solid surface (coating) can be achieved by removing the solid from a liquid bath at a constant velocity V [Kistler and Schweizer (1997), Quéré (1999)].

When the solid reduces to a flat plate [figure 1-(a)], the thickness h_∞ of the extracted film has first been studied experimentally [Goucher and Ward (1922), Morey (1940)], and has led to the LLD theory [Landau and Levich (1942), Derjaguin (1943)] which gives (see section 4.2):

$$h_\infty = 0,94.a.Ca^{2/3}, \qquad (1.1)$$

where $a \equiv \sqrt{\sigma/\rho g}$ is the capillary length and $Ca \equiv \mu V/\sigma$ the capillary number. The above expression holds in the low capillary limit $Ca \ll 1$, where the pressure at the interface mainly depends on surface tension. To reach the law (1.1), one must consider the role of the liquid meniscus which imposes, via curvature effects, a constant film thickness at the exit of the bath. In this sense, one can say that the meniscus acts as a "liquid wiper".

The problem we address is to find the law for h_∞, when the capillary wiper is replaced by an elastic sheet wiper [figure 1-(b)].

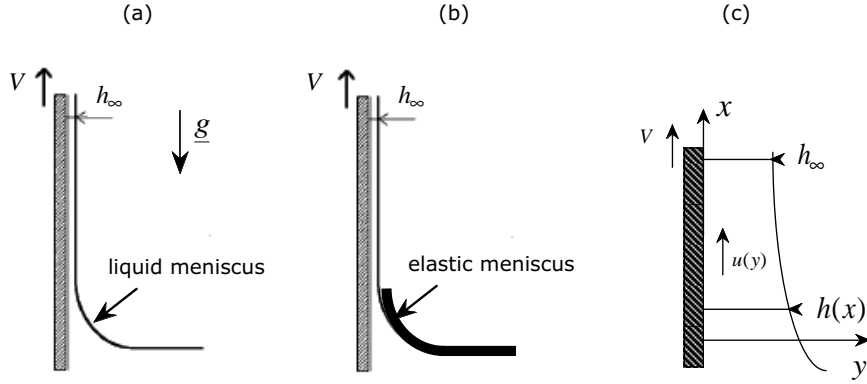The experimental set-up is presented in section 2, the results in section 3 and the model in section 4.

FIGURE 1. Plate coatings (a) through a capillary meniscus (b) through an elastic sheet (c) conventions used to describe the coating problem.

thickness h_s μm	density ρ_s kg.m^{-3}	bending stiffness B kg.m^2.s^{-2}	Young modulus $E \equiv 12\left(1-\nu^2\right)B/h_s^3$ GPa	$\mathcal{L}$ cm
55	1280	57.10^{-6}	3.7	4.3
75	1344	162.10^{-6}	4.0	5.4
100	1387	354.10^{-6}	3.7	6.3
150	1337	795.10^{-6}	2.5	7.3
180	1338	1232.10^{-6}	2.2	8.0
490	906	10 041.10^{-6}	0.9	13.1

TABLE 1. Physical properties of the different mylar sheets.

2. Experimental set-up and protocol

The experimental set-up is presented on figure 2-(a): the elastic sheet of length L and width b (1) is clamped on a support (2) at a distance y_0 from the solid support to be coated (3).

The physical properties of the mylar sheets we have used are reported on table 1. Apart from the sheet thickness h_s and density ρ_s, we present on table 1 the measured values of the bending stiffness per unit width B and the deduced value of the Young modulus $E \equiv 12\left(1-\nu^2\right)B/h_s^3$. In this expression, the Poisson ratio is taken constant $\nu = 1/3$. The last column presents the value of the characteristic length $\mathcal{L} \equiv [B/(\rho_s.h_s.g)]^{1/3}$ under which gravity does not affect the equilibrium shape of the sheet. The whole study is conducted in the limit $L/\mathcal{L} < 1$, where gravity can be neglected to describe the shape of the sheet of length L.

The liquid (silicone oil) is chosen to wet both the elastic sheet and the solid support. It is initially deposited with a micropipet between the sheet and the solid surface as presented on figure 2-(b). The deposited volume Ω is of the order of 1000 μl and we always manage to keep it to a value much larger than the coating volume. In this limit, there is no influence of Ω on the deposited film thickness as will be shown in section 3. The physical properties of the silicone oils used (S.O.) are presented on table 2.

Once the liquid is deposited, the solid support is moved at a constant velocity in the

Liquid	ρ kg m^{-3}	μ kg m^{-1} s^{-1}	σ N m^{-1}	a m
S.O. V100	952	0.1	0,0225	1,6 10^{-3}
S.O. V1000	965	1	0,0225	1,5 10^{-3}

TABLE 2. Physical properties of the different Newtonian liquids used (at 25°C).
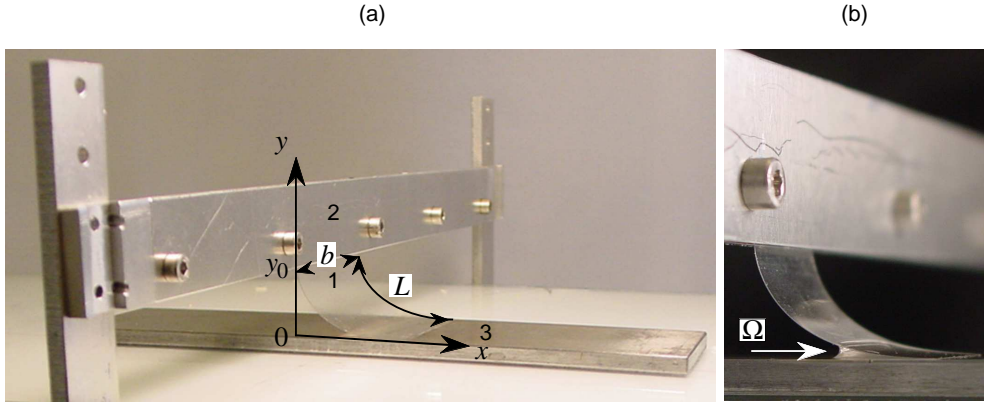
FIGURE 2. Experimental set-up: (a) general view showing the elastic plate (1), its clamping support (2) and the coated solid plate (3). (b) close view on the elastic plate and the liquid reservoir of volume Ω.
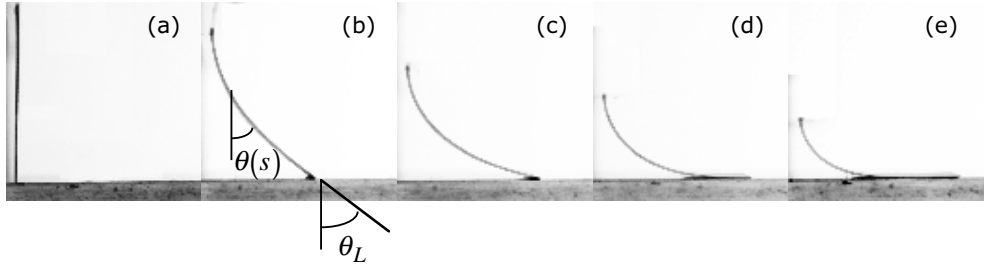
FIGURE 3. Shape of the elastic sheet obtained with $L = 28.5$ mm, $h_s = 100$ μm and : (a) $y_0/L = 1$, $\theta_L = 0°$ (b) $y_0/L = 0.8$, $\theta_L = 52°$ (c) $y_0/L = 0.6$, $\theta_L = 75°$ (d) $y_0/L = 0.44$, $\theta_L = 90°$ (e) $y_0/L = 0.3$, $\theta_L = 90°$.

direction of positive x. The velocity is controlled by a step motor (Cool Muscle, CM1 series) and can be varied from 100 μm/s to 14 cm/s.

After the coating of the whole surface, the solid is weighted and we deduce from the difference of mass before and after deposition, the value of the mean thickness h_∞.

3. Experimental results

3.1. *Influence of the reduced distance y_0/L.*

The shape of the elastic sheet is presented on figure 3 for different values of the reduced solid surface distance y_0/L. We observe on this figure that the angle at the end of the sheet θ_L increases from 0 at $y_0/L = 1$ to $\pi/2$ at $y_0/L = 0.44$. For smaller values of the
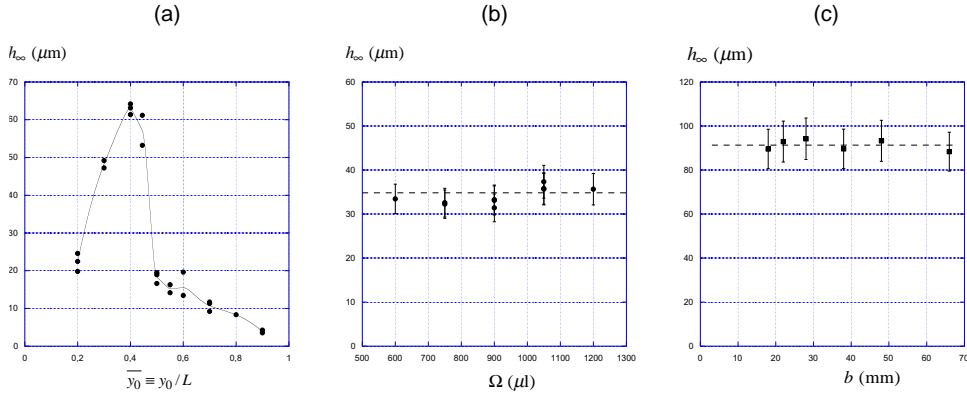
FIGURE 4. Experimental results : (a) Influence of the reduced distance y_0/L on the film thickness h_∞ obtained with V100, $V = 28.8$ mm/s, $b = 38$ mm, $L = 28.5$ mm, $h_s = 180$ μm. (b) Influence of the reservoir volume Ω obtained with V100, $V = 12$ mm/s, $b = 3.8$ cm, $y_0/L = 0.44$, $L = 45.5$ mm and $h_s = 100$ μm (c) Influence of the sheet width b obtained with V100, $V = 28.8$ mm/s, $y_0/L = 0.44$, $L = 35.5$ mm, $h_s = 100$ μm.

reduced distance, this angle remains equal to $\pi/2$ and the horizontal fraction of the sheet length increases, as well as its initial curvature.

The evolution of the film thickness h_∞ with the reduced distance y_0/L is presented on figure 4-(a). This evolution presents a maximum for $y_0/L \approx 0.4 - 0.45$, that is when the sheet gets in contact with the solid with a $\pi/2$ contact angle θ_L [see figure 3-(d)] and with almost a zero contact surface . The whole study is conducted in the limit $y_0/L = 0.44$.

3.2. *Influence of the reservoir volume Ω.*

The influence of the volume of the reservoir Ω [figure 2-(b)] on the film thickness h_∞ is presented on figure 4-(b). These measurements have been performed with V100, $V = 12$ mm/s, $b = 38$ mm, $y_0 = 0.44$, $L = 45.5$ mm and $h_s = 100$ μm.

We observe on this figure that within the experimental error on the measure of h_∞ (of the order of $\pm 10\%$) the film thickness is independent of the volume of the reservoir.

3.3. *Influence of the sheet width b.*

The evolution of the film thickness h_∞ with the sheet width b is presented on figure 4-(c): Within the experimental error on the measurement of h_∞ (10%) the film thickness is independent of the width b.

3.4. *Influence of the velocity V and viscosity μ.*

The evolution of the film thickness h_∞ with the velocity is presented on figure 5-(a): the thickness of the coating increases with V as a power law $h_\infty \sim V^\alpha$ with $\alpha \approx 3/4$. We also observe on this figure that the thickness increases with the viscosity of the liquid: using a silicone oil ten times more viscous (V1000 instead of V100) leads to a thickness ten times larger.

3.5. *Influence of the sheet length L.*

The evolution of the film thickness h_∞ with the sheet length L is presented on figure 5-(b): in these experiments, all the parameters are kept constant (in particular the ratio y_0/L) except the length L. We observe a strong power law dependency of the film thickness $h_\infty \sim L^\beta$ with $\beta \approx 5/2$.
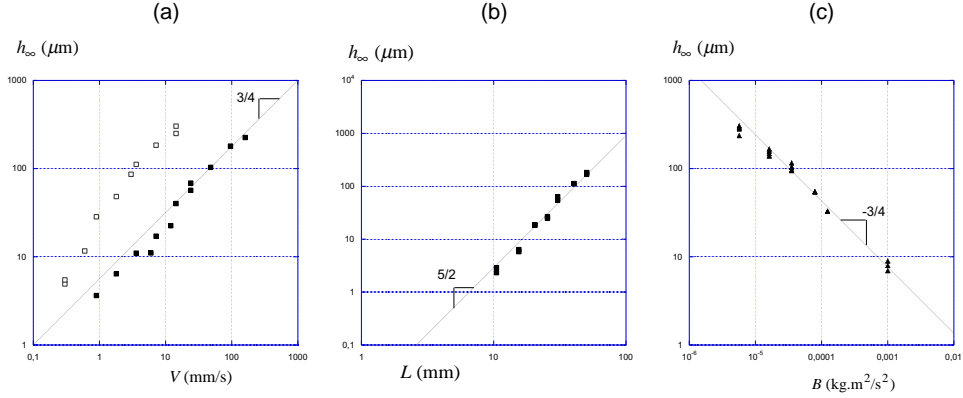
FIGURE 5. Experimental results : (a) Influence of the velocity V obtained with V100 (■) and V1000 (□) using the elastic sheet defined by $b = 38$ mm, $y_0/L = 0.44$, $L = 35.5$ mm and $h_s = 100$ μm. (b) Influence of the sheet length L obtained with V100, $V = 28.8$ mm/s, $b = 38$ mm, $y_0/L = 0.44$, and $h_s = 100$ μm (c) Influence of the sheet bending stiffness B obtained with V100, $V = 28.8$ mm/s, $b = 38$ mm, $y_0/L = 0.44$, $L = 55.5$ mm.

3.6. *Influence of the sheet bending stiffness B.*

The influence of the sheet bending stiffness B is presented on figure 5-(c): again, all the parameters are kept constant except B which is varied using the different mylar sheets presented on table 1. We observe on this figure that the coating thickness h_∞ decreases with B following a power law $h_\infty \sim B^\gamma$ with $\gamma \approx -3/4$.

4. Model

In this section, we first present some scaling arguments intended to capture the physical skeleton which sustains the delicate LLD theory [Landau and Levich (1942), Derjaguin (1943)]. This theory is then more deeply presented and in a second step adapted to the coating by an elastic sheet.

4.1. *Some scaling arguments*

The idea developed by Landau, Levich and Derjaguin to reach the expression of h_∞ in the case of plate coating [figure 1-(a)] is to consider the liquid motion in a region located in between the liquid meniscus (where the fluid is mainly at rest) and the film region (where the liquid mainly move at the velocity of the wall). In this intermediate region (of vertical extension λ), the motion of the fluid must satisfy (in the low Reynolds number limit) the Stokes equation which can be dimensionally written :

$$\mu \frac{V}{h_\infty^2} \sim \sigma \frac{h_\infty}{\lambda^3} \tag{4.1}$$

where $\sigma\, h_\infty/\lambda^3$ represents the gradient of the capillary pressure. This equation states that the liquid is entrained by viscosity and retained by surface tension. The value of the thickness h_∞ results from this equilibrium. To evaluate the gradient of the capillary pressure, the idea is that the value of the curvature changes from 0 in the film region to $1/a$ in the meniscus region over the distance λ: $h_\infty/\lambda^3 \sim 1/(\lambda\, a)$. This matching of the two zones leads to the scaling of the film thickness:

$$h_\infty \sim a\, Ca^{2/3} \tag{4.2}$$

If one transposes this approach to the problem of the elastic meniscus, the first modification lies in the expression of the pressure gradient:

$$\mu \frac{V}{h_\infty^2} \sim B \frac{h_\infty}{\lambda^5} \tag{4.3}$$

The second difference lies in the matching which is done here on the force (instead of the pressure) and leads to the evaluation of $\lambda : h_\infty / \lambda^3 \sim 1/L^2$. As for the LLD problem, the Stokes equation and the matching condition with the unperturbed meniscus provides the scaling for the film thickness:

$$h_\infty \sim L\, Ce^{3/4} \quad \text{where} \quad Ce \equiv \frac{\mu V L^2}{B} \tag{4.4}$$

4.2. *The LLD theory.*

The problem of dragging a liquid by an upward moving vertical plate [figure 1-(a)] is discussed using the conventions presented in figure 1-(c).

We describe the flow in the "small slope region" ($h_x \equiv dh/dx \ll 1$), where we assume that the velocity is mainly aligned with x and mainly depends on y ($\underline{U} \approx u(y)\underline{e}_x$). We don't know exactly where this region is but we are sure that it exists by continuity between the zero slope region ($h = h_\infty$) located at $x = +\infty$ and the infinite slope region located at the junction with the bath $x = -\infty$.

In this small slope region the conservation of mass imposes

$$h \langle u \rangle = h_\infty \langle u \rangle_\infty \tag{4.5}$$

where $\langle u \rangle$ is the mean velocity defined by $h \langle u \rangle = \int_0^h u(y)dy$.

In the limit of small Reynolds number $Re \approx V h_\infty / \nu$ the steady motion of the Newtonian liquid is described by the Stokes equation:

$$\mu \Delta \underline{U} = \underline{\text{grad}}p - \rho \underline{g} \tag{4.6}$$

Along the y direction, this equation reduces to $\partial p / \partial y = 0$ which states that the pressure at any x location can be deduced from its value at the interface [$y = h(x)$] where the continuity of stresses imposes:

$$-p.\underline{n} + \left(\underline{\underline{\tau}}.\underline{n}\right) = -p_0.\underline{n} + \sigma.C.\underline{n}. \tag{4.7}$$

Here p_0 is the pressure in the surrounding gas, $\underline{n}$ the outward normal vector, $\underline{\underline{\tau}} \equiv \mu \left(\underline{\text{grad}}\,\underline{U} +^T \underline{\text{grad}}\,\underline{U}\right)$ the fluid stress tensor and C the curvature of the interface which imposes the Laplace pressure jump. In the limit of small capillary number $Ca \equiv \mu V / \sigma \ll 1$, the pressure jump at the interface is mainly related to the capillary effect and the above equation (4.7) reduces to $p = p_0 - \sigma h_{xx}$ along the normal $\underline{n}$ and to $\partial u / \partial y = 0$ along the tangential direction. This expression of the pressure in the liquid enables the integration of the equation of motion (4.6) along the x direction, which leads to:

$$h \langle u \rangle = hV - \frac{h^3}{3\nu}\left(g - \frac{\sigma}{\rho}h_{xxx}\right) \tag{4.8}$$

Using h_∞ to scale the film thickness ($\bar{h} \equiv h/h_\infty$) and $\mathcal{L}_x \equiv h_\infty / (3Ca)^{1/3}$ to scale the lengths along the x direction ($\bar{x} \equiv x/\mathcal{L}_x$), the above equation (4.8) becomes, using (4.5):

$$\bar{h}^3 \bar{h}_{\bar{x}\bar{x}\bar{x}} = 1 - \bar{h} + \left(\frac{h_\infty}{a}\right)^2 \frac{1}{3Ca}\left(\bar{h}^3 - 1\right) \tag{4.9}$$

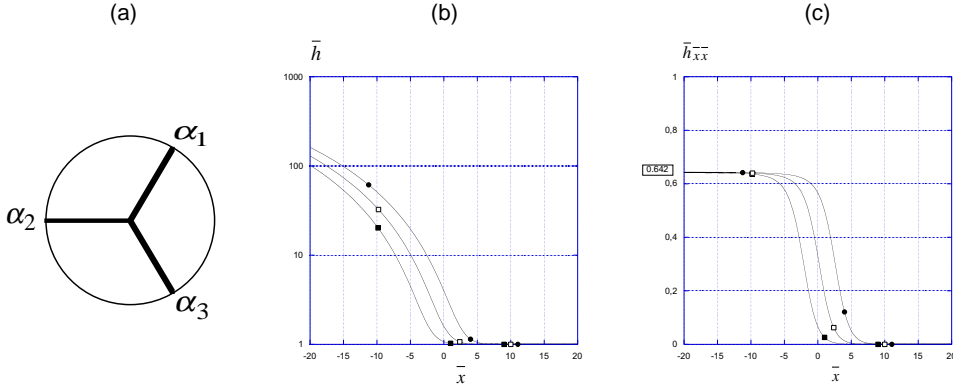The last term in equation (4.9) represents the effect of gravity. Since we will show that

FIGURE 6. (a) visualisation on the unit circle of the three solutions of the equation $\alpha_i^3 = -1$. (b) evolution of the reduced thickness $\bar{h}(\bar{x})$ obtained through the numerical integration of equation (4.10) with different values of the constant A: $A = 0.1$ (■), $A = 1$ (□) and $A = 10$ (●). (c) evolution of the reduced curvature $\bar{h}_{\bar{x}\bar{x}}(\bar{x})$ obtained through the numerical integration of equation (4.10) with different values of the constant A: $A = 0.1$ (■), $A = 1$ (□) and $A = 10$ (●).

$h_\infty/a \sim Ca^{2/3}$, this term is of order $Ca^{1/3} \ll 1$ compared to the entrainment term and the capillary term. The motion of the liquid is thus governed by the parameter free equation:

$$\frac{d}{d\bar{x}}\bar{h}_{\bar{x}\bar{x}} = \frac{1 - \bar{h}}{\bar{h}^3} \tag{4.10}$$

which must be integrated with the limit condition $\bar{h}(\bar{x} = +\infty) = 1$. In this quasi-constant thickness region we seek an asymptotic solution under the form $\bar{h}(\bar{x}) = 1 + \epsilon(\bar{x})$. According to equation (4.10), the function $\epsilon(\bar{x})$ must satisfy the linear equation $\epsilon_{\bar{x}\bar{x}\bar{x}} = -\epsilon$. We deduce that $\epsilon(\bar{x}) = A_i e^{\alpha_i \bar{x}}$, where $\alpha_i^3 = -1$. The three solutions of this equation are presented on figure 6-(a). Two of them (α_1 and α_3) have positive real part and thus diverge in $\bar{x} = +\infty$. The vanishing condition impose $\epsilon(\bar{x}) = A_2 e^{\alpha_2 \bar{x}} = A e^{-\bar{x}}$. This asymptotic function is used to impose the three initial conditions which are needed to integrate equation (4.10). The results of the numerical integration of this equation are presented on figures 6-(b) for $\bar{h}(\bar{x})$ and -(c) for $\bar{h}_{\bar{x}\bar{x}}(\bar{x})$ using three different values of the constant A (0.1, 1 and 10). We observe on figure 6-(b) that the film thickness increases when $\bar{x} \to -\infty$. As expected, this increase occurs sooner with high values of A. This free parameter A is related to the fuzzy location of the small slope region. It does not change the main characteristic of equation (4.10) which states that he curvature $\bar{h}_{\bar{x}\bar{x}}$ becomes constant when $\bar{h}$ goes to infinity. Figure 6-(c) shows that this constant is independant of A and equals 0.642.

In the limit $\bar{x} \to -\infty$, the small slope region much connect the meniscus region. The above property of the Stokes equation suggests that the constant curvature obtained in this limit must be equal to the curvature of the meniscus in the region of small slope, that is at the contact with the wall. This static meniscus curvature is known since the work of Laplace [Clanet and Quéré (2002)] and is equal to $\sqrt{2}/a$ at the wall. The matching of curvatures between both regions thus writes:

$$\frac{h_\infty}{\mathcal{L}_x^2}\bar{h}_{\bar{x}\bar{x}} = \frac{\sqrt{2}}{a} \tag{4.11}$$

which finally leads to $h_\infty = 0,94.a.Ca^{2/3}$.

4.3. *Theory for the coating by an elastic sheet.*

The theoretical approach we use to evaluate the film thickness h_∞ deposited by an elastic membrane is similar to the LLD theory: We first focus on the flow in the small slope region and then consider the matching with the shape of the elastic meniscus.

Concerning the flow in the small slope region, the equation of mass (4.5) remains unchanged whereas the equation of Stokes simplifies:

$$\mu \Delta \underline{U} = \underline{\text{grad}} p \tag{4.12}$$

We work here in the low gravity limit $\rho g h_\infty^2 / \mu V \ll 1$. The pressure is deduced from the continuity of stresses at the solid-liquid interface, the projection of which along the normal $\underline{n}$ writes in the stationnary limit [Hosoi and Mahadevan (2004)]:

$$-p + \left(\underline{\underline{\tau}} . \underline{n}\right) . \underline{n} = \frac{Eb\left(1 - \nu\right)}{\left(1 + \nu\right)\left(1 - 2\nu\right)} \gamma h_{xx} - B h_{xxxx} \tag{4.13}$$

where γ is the in-plane elastic strain, $B h_{xxxx}$ the bending contribution. In the working domain, the mylar sheets we use do not experience any elongation and we thus take the limit $\gamma = 0$. In this limit, the pressure at the solid-liquid interface reduces to $p = B.h_{xxxx}$ (instead of $p = p_0 - \sigma.h_{xx}$ for the LLD problem). This expression for the pressure, together with the zero velocity condition at the membrane, enables the integration of the Stokes equation (4.12) along the x direction, which leads to:

$$h \langle u \rangle = \frac{1}{2} h V - \frac{B}{12\mu} h^3 h_{xxxxx} \tag{4.14}$$

Using h_∞ to scale the thickness and $\mathcal{L}_{xe} = h_\infty / Ce^{1/5}$ ($Ce \equiv 6\mu V h_\infty^2 / B$) to scale the lengths along the x direction, we obtain the nondimensional (and parameter free) version of equation (4.14):

$$\frac{d}{d\bar{x}} \bar{h}_{\bar{x}\bar{x}\bar{x}\bar{x}} = \frac{\bar{h} - 1}{\bar{h}^3} \tag{4.15}$$

This equation is "similar" to the one obtained in the LLD theory (4.10) and must be solved with the same limit condition : $\bar{h}(\bar{x} = +\infty) = 1$. Looking for an asymptotic function $\bar{h}(\bar{x}) = 1 + \epsilon(\bar{x})$, we get $\epsilon(\bar{x}) = A_i e^{\alpha_i \bar{x}}$, where $\alpha_i^5 = +1$. Among the five solutions of this equation presented on figure 7-(a), only two (α_3 and α_4) lead to vanishing function at $\bar{x} = +\infty$. The asymptotic function for $\bar{h}(\bar{x})$ thus writes: $\bar{h}(\bar{x}) = 1 + A.e^{\cos(4\pi/5).\bar{x}} . \cos[\sin(4\pi/5).\bar{x}] + B.e^{\cos(4\pi/5).\bar{x}} . \sin[\sin(4\pi/5).\bar{x}]$, where A and B are two constants. This asymptotic function is used to provide the five initial conditions needed to integrate equation (4.15). The evolution of the film thickness $\bar{h}(\bar{x})$ obtained by numerical integration is presented on figure 7-(b), for different couples of constant A and B. In the limit $\bar{x} \to -\infty$, the thickness of the film increases and we deduce from equation (4.15) that the reduced fourth derivative $\bar{h}_{\bar{x}\bar{x}\bar{x}\bar{x}}$ must become constant. As for the LLD problem, the value of this constant must be deduced by matching with the shape of the elastic meniscus.

The elastic meniscus is described by the Elastica equation [Landau and Lifchitz (1967)]:

$$\frac{d^2\theta}{ds^2} = -\frac{F}{B} \sin\theta \tag{4.16}$$

where $\theta(s)$ is the local angle presented on figure 3-(b), s the curvilinear coordinate ($s = 0$ at the clamping location) and F is the intensity of the force exerted by the solid surface on the elastic sheet (by unit width). Equation (4.16) must be solved with the two limit conditions: $\theta(s = 0) = 0$ and $d\theta/ds(s = L) = 0$. This integration shows that F is related
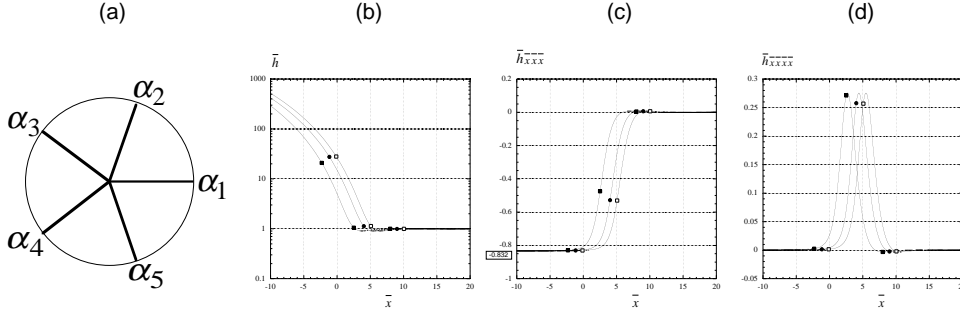
FIGURE 7. (a) visualisation on the unit circle of the five solutions of the equation $\alpha_i^5 = +1$. (b) evolution of the reduced thickness $\bar{h}(\bar{x})$ obtained through the numerical integration of equation (4.15) with different values of the constants A and B: $A = 3.355$, $B = 0$ (■), $A = 0$, $B = 29.267$ (□) and $A = 7.803$, $B = 10$ (●). (c) evolution of the reduced third derivative $\bar{h}_{\bar{x}\bar{x}\bar{x}}(\bar{x})$ obtained through the numerical integration of equation (4.15) with different values of the constants A and B: $A = 3.355$, $B = 0$ (■), $A = 0$, $B = 29.267$ (□) and $A = 7.803$, $B = 10$ (●). (d) evolution of the reduced fourth derivative $\bar{h}_{\bar{x}\bar{x}\bar{x}\bar{x}}(\bar{x})$ obtained through the numerical integration of equation (4.10) with different values of the constant A: $A = 0.1$ (■), $A = 1$ (□) and $A = 10$ (●).

to the reduced distance y_0/L and for $y_0/L = 0.44$, we find $F = 3, 43. B/L^2$. In this limit, where $\theta(L) = \pi/2$), we observe that equation (4.16) can be expanded in $s = L$ as: $h_{xxx} = -F/B$ and $h_{xxxx} = 0$. The constant for the matching is thus null and the free parameters A and B must be chosen to verify this condition. This condition is fulfilled for the three couples used to integrate numerically equation (4.15), as shown on figure 7-(d).

Since $h_{xxxx} = 0$, one deduces that h_{xxx} is constant and the matching can be done on the third derivative. According to figure 7-(c) the limit $\bar{h}_{\bar{x}\bar{x}\bar{x}} = -0.832$ and the matching with the Elastica gives:

$$-0.832 \frac{h_\infty}{\mathcal{L}_{xe}^3} = -\frac{3.43}{L^2} \tag{4.17}$$

From which we deduce:

$$h_\infty = 0,65. \, L \, \left(\frac{\mu V L^2}{B} \right)^{3/4} \tag{4.18}$$

The comparison between the measured thickness h_∞ and the theoretical characteristic length $L. \left(\mu V L^2/B \right)^{3/4}$ is shown on figure 8 for all the different experimental conditions presented on figures 5. We observe that the measured thickness is a linear function of the theoretical thickness with a coefficient of proportionality of 0.065, different from the 0.65 expected from equation (4.18). This difference comes from the fact that we have assumed in our model that all the liquid entrained by the solid surface goes into the coating film. The experiments tell us that this is not the case and that some recirculation must take place in the reservoir.

5. Conclusion

We have conducted a series of experiments on the coating of a flat solid surface by an elastic sheet. Experimentally, we show that the film thickness, h_∞, is very sensitive to the shape of the membrane [figure 4-(a)]. For a fixed shape ($y_0/L = 0.44$), we show that the thickness follows the law $h_\infty \approx 0.065 L \, Ce^{3/4}$, where $Ce \equiv \mu.V.L^2/B$. Theoretically, we
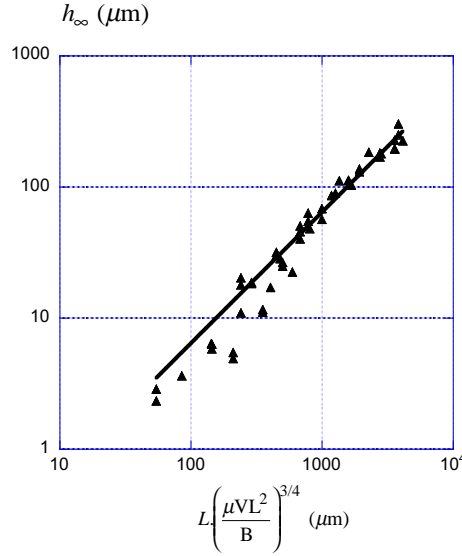
h_∞ (μm)

FIGURE 8. Evolution of the film thickness h_∞ as a function of the characteristic length scale $L.(\mu.V.L^2/B)^{3/4}$: experimental points presented in figures 5 (■), best fit (solid line) $h_\infty = 0.065L.Ce^{3/4}$.

recover this scaling through an extension of the LLD theory and show that the maximal film thickness is $h_\infty = 0.65L\ Ce^{3/4}$. The recirculation in the region in front of the wiper must be considered to reach the experimental prefactor.

REFERENCES

CLANET, C. AND QUERE, D. 2002 Onset of menisci. *J.Fluid Mech.* **460**, 131–149

DERJAGUIN B.V. 1943 On the thickness of the liquid film adhering to the walls of a vessel after emptying. *Acta Physicochim. USSR* **20**, 349–52.

GOUCHER F.S., WARD H. 1922 The thickness of liquid films formed on solid surfaces under dynamic condition. *Phil. Mag.* **44**, 1002–1014.

HOSOI A.E. AND MAHADEVAN L. 2004 Peeling, healing, and bursting in a lubricated elastic sheet. *Phys. Rev. Lett.* **93**, 137802.

KISTLER S.F. AND SCHWEIZER P.M. 1997 Liquid Film Coating *Chapman & Hal*

KORB D.R., HERMAN J.P., GREINER J.V., SCAFFIDI R.C., FINNEMORE V.M., EXFORD J.M., BLACKIE C.A. AND DOUGLASS T. 2005 Lid wiper epitheliopathy and dry eye symptoms. *Eye Contact Lens* **31**, 2–8.

LANDAU L. AND LIFCHITZ E. 1967 Theory of elasticity. *Editions Mir, Moscou*

QUÉRÉ D. 1999 Fluid coating on a fiber. *Annu. Rev. Fluid Mech.* **31**, 347–84.

KITZIO J.P., KAMOTANI Y. AND OSTRACH S. 1999 free coating flows at high capillary and Reynolds number. *Exp. Fluid.* **27**, 235–43.

LANDAU L.D., LEVICH B. 1942 Dragging of a liquid by a moving plate. *Acta Physicochim. USSR* **17**, 42–54.

MOREY FC. 1940 Thickness of a film adhering to a surface slowly withdrawn from the liquid. *J. Res. Natl. Bur. Stand.* **25**, 385–93.